Pergamon

Carbon, Vol. 33, No. 7, pp. 883–891, 1995

0008-6223/95 $9.50 + .00

0008-6223(95)00017-8

PHYSICS OF CARBON NANOTUBES

M. S. DRESSELHAUS,[1] G. DRESSELHAUS,[2] and R. SAITO[3]
[1]Department of Electrical Engineering and Computer Science and Department of Physics, Massachusetts Institute of Technology, Cambridge, Massachusetts 02139, U.S.A.
[2]Francis Bitter National Magnet Laboratory, Massachusetts Institute of Technology, Cambridge, Massachusetts 02139, U.S.A.
[3]Department of Electronics-Engineering, University of Electro-Communications, Tokyo 182, Japan

(*Received* 26 *October* 1994; *accepted* 10 *February* 1995)

Abstract—The fundamental relations governing the geometry of carbon nanotubes are reviewed, and explicit examples are presented. A framework is given for the symmetry properties of carbon nanotubes for both symmorphic and non-symmorphic tubules which have screw-axis symmetry. The implications of symmetry on the vibrational and electronic structure of 1D carbon nanotube systems are considered. The corresponding properties of double-wall nanotubes and arrays of nanotubes are also discussed.

Key Words—*Single-wall, multi-wall, vibrational modes, chiral nanotubes, electronic bands, tubule arrays.*

1. INTRODUCTION

Carbon nanotube research was greatly stimulated by the initial report of observation of carbon tubules of nanometer dimensions[1] and the subsequent report on the observation of conditions for the synthesis of large quantities of nanotubes[2,3]. Since these early reports, much work has been done, and the results show basically that carbon nanotubes behave like rolled-up cylinders of graphene sheets of sp^2 bonded carbon atoms, except that the tubule diameters in some cases are small enough to exhibit the effects of one-dimensional (1D) periodicity. In this article, we review simple aspects of the symmetry of carbon nanotubules (both monolayer and multilayer) and comment on the significance of symmetry for the unique properties predicted for carbon nanotubes because of their 1D periodicity.

Of particular importance to carbon nanotube physics are the many possible symmetries or geometries that can be realized on a cylindrical surface in carbon nanotubes without the introduction of strain. For 1D systems on a cylindrical surface, translational symmetry with a screw axis could affect the electronic structure and related properties. The exotic electronic properties of 1D carbon nanotubes are seen to arise predominately from intralayer interactions, rather than from interlayer interactions between multilayers within a single carbon nanotube or between two different nanotubes. Since the symmetry of a single nanotube is essential for understanding the basic physics of carbon nanotubes, most of this article focuses on the symmetry properties of single layer nanotubes, with a brief discussion also provided for two-layer nanotubes and an ordered array of similar nanotubes.

2. FUNDAMENTAL PARAMETERS AND RELATIONS FOR CARBON NANOTUBES

In this section, we summarize the fundamental parameters for carbon nanotubes, give the basic relations governing these parameters, and list typical numerical values for these parameters.

In the theoretical carbon nanotube literature, the focus is on single-wall tubules, cylindrical in shape with caps at each end, such that the two caps can be joined together to form a fullerene. The cylindrical portions of the tubules consist of a single graphene sheet that is shaped to form the cylinder. With the recent discovery of methods to prepare single-walled nanotubes[4,5], it is now possible to test the predictions of the theoretical calculations.

It is convenient to specify a general carbon nanotubule in terms of the tubule diameter d_t and the chiral angle θ, which are shown in Fig. 1. The chiral vector $\mathbf{C}_h$ is defined in Table 1 in terms of the integers (n,m) and the basis vectors $\mathbf{a}_1$ and $\mathbf{a}_2$ of the honeycomb lattice, which are also given in the table in terms of rectangular coordinates. The integers (n,m) uniquely determine d_t and θ. The length L of the chiral vector $\mathbf{C}_h$ (see Table 1) is directly related to the tubule diameter d_t. The chiral angle θ between the $\mathbf{C}_h$ direction and the zigzag direction of the honeycomb lattice $(n,0)$ (see Fig. 1) is related in Table 1 to the integers (n,m).

We can specify a single-wall C_{60}-derived carbon nanotube by bisecting a C_{60} molecule at the equator and joining the two resulting hemispheres with a cylindrical tube having the same diameter as the C_{60} molecule, and consisting of the honeycomb structure of a single layer of graphite (a graphene layer). If the C_{60} molecule is bisected normal to a five-fold axis, the "armchair" tubule shown in Fig. 2 (a) is formed, and if the C_{60} molecule is bisected normal to a 3-fold axis, the "zigzag" tubule in Fig. 2(b) is formed[6]. Armchair and zigzag carbon nanotubules of larger diameter, and having correspondingly larger caps, can likewise be defined, and these nanotubules have the general appearance shown in Figs. 2(a) and (b). In addition, a large number of chiral carbon nanotubes can be formed for $0 < |\theta| < 30°$, with a screw axis along

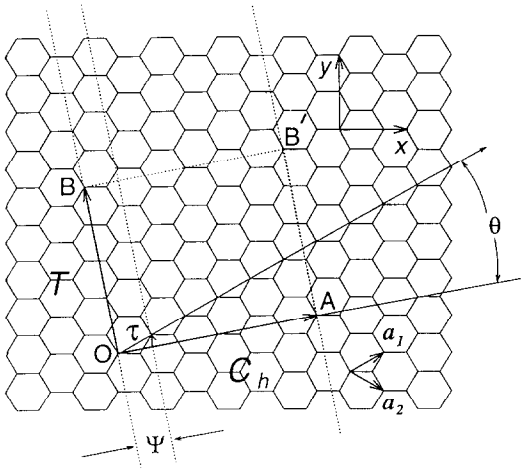

Fig. 1. The 2D graphene sheet is shown along with the vector which specifies the chiral nanotube. The chiral vector **OA** or $\mathbf{C}_h = n\boldsymbol{a}_1 + m\boldsymbol{a}_2$ is defined on the honeycomb lattice by unit vectors $\boldsymbol{a}_1$ and $\boldsymbol{a}_2$ and the chiral angle θ is defined with respect to the zigzag axis. Along the zigzag axis $\theta = 0°$. Also shown are the lattice vector **OB** = **T** of the 1D tubule unit cell, and the rotation angle ψ and the translation τ which constitute the basic symmetry operation $R = (\psi|\tau)$. The diagram is constructed for $(n,m) = (4,2)$.

the axis of the tubule, and with a variety of hemispherical caps. A representative chiral nanotube is shown in Fig. 2(c).

The unit cell of the carbon nanotube is shown in Fig. 1 as the rectangle bounded by the vectors $\mathbf{C}_h$ and **T**, where **T** is the 1D translation vector of the nanotube. The vector **T** is normal to $\mathbf{C}_h$ and extends from

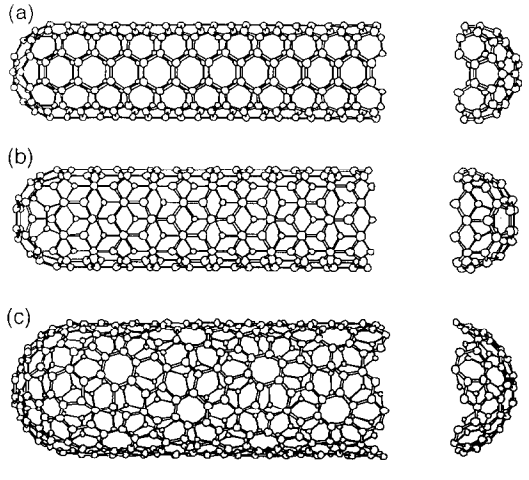

Fig. 2. By rolling up a graphene sheet (a single layer of carbon atoms from a 3D graphite crystal) as a cylinder and capping each end of the cylinder with half of a fullerene molecule, a "fullerene-derived tubule," one layer in thickness, is formed. Shown here is a schematic theoretical model for a single-wall carbon tubule with the tubule axis OB (see Fig. 1) normal to: (a) the $\theta = 30°$ direction (an "armchair" tubule), (b) the $\theta = 0°$ direction (a "zigzag" tubule), and (c) a general direction B with $0 < |\theta| < 30°$ (a "chiral" tubule). The actual tubules shown in the figure correspond to (n,m) values of: (a) (5,5), (b) (9,0), and (c) (10,5).

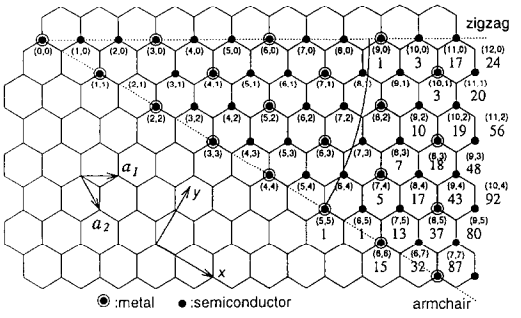

Fig. 3. The 2D graphene sheet is shown along with the vector which specifies the chiral nanotube. The pairs of integers (n,m) in the figure specify chiral vectors $\mathbf{C}_h$ (see Table 1) for carbon nanotubes, including zigzag, armchair, and chiral tubules. Below each pair of integers (n,m) is listed the number of distinct caps that can be joined continuously to the cylindrical carbon tubule denoted by (n,m)[6]. The circled dots denote metallic tubules and the small dots are for semiconducting tubules.

the origin to the first lattice point **B** in the honeycomb lattice. It is convenient to express **T** in terms of the integers (t_1, t_2) given in Table 1, where it is seen that the length of **T** is $\sqrt{3}L/d_R$ and d_R is either equal to the highest common divisor of (n,m), denoted by d, or to $3d$, depending on whether $n - m = 3dr$, r being an integer, or not (see Table 1). The number of carbon atoms per unit cell n_c of the 1D tubule is $2N$, as given in Table 1, each hexagon (or unit cell) of the honeycomb lattice containing two carbon atoms.

Figure 3 shows the number of distinct caps that can be formed theoretically from pentagons and hexagons, such that each cap fits continuously on to the cylinders of the tubule, specified by a given (n,m) pair. Figure 3 shows that the hemispheres of C_{60} are the smallest caps satisfying these requirements, so that the diameter of the smallest carbon nanotube is expected to be 7 Å, in good agreement with experiment[4,5]. Figure 3 also shows that the number of possible caps increases rapidly with increasing tubule diameter.

Corresponding to selected and representative (n,m) pairs, we list in Table 2 values for various parameters enumerated in Table 1, including the tubule diameter d_t, the highest common divisors d and d_R, *the length* L of the chiral vector $\mathbf{C}_h$ in units of a (where a is the length of the 2D lattice vector), the length of the 1D translation vector **T** of the tubule in units of a, and the number of carbon hexagons per 1D tubule unit cell N. Also given in Table 2 are various symmetry parameters discussed in section 3.

3. SYMMETRY OF CARBON NANOTUBES

In discussing the symmetry of the carbon nanotubes, it is assumed that the tubule length is much larger than its diameter, so that the tubule caps can be neglected when discussing the physical properties of the nanotubes.

The symmetry groups for carbon nanotubes can be either symmorphic [such as armchair (n,n) and zigzag

Table 1. Parameters of carbon nanotubes

Symbol	Name	Formula	Value
$a_{C\text{-}C}$	carbon-carbon distance		1.421 Å (graphite)
a	length of unit vector	$\sqrt{3}a_{C\text{-}C}$	2.46 Å
$\mathbf{a}_1, \mathbf{a}_2$	unit vectors	$\left(\frac{\sqrt{3}}{2}, \frac{1}{2}\right)a, \left(\frac{\sqrt{3}}{2}, -\frac{1}{2}\right)a$	in (x,y) coordinates
$\mathbf{b}_1, \mathbf{b}_2$	reciprocal lattice vectors	$\left(\frac{1}{\sqrt{3}}, 1\right)\frac{2\pi}{a}, \left(\frac{1}{\sqrt{3}}, -1\right)\frac{2\pi}{a}$	in (x,y) coordinates
$\mathbf{C}_h$	chiral vector	$\mathbf{C}_h = n\mathbf{a}_1 + m\mathbf{a}_2 \equiv (n,m)$	n,m: integers
L	circumference of nanotube	$L = \lvert\mathbf{C}_h\rvert = a\sqrt{n^2 + m^2 + nm}$	$0 \le \lvert m\rvert \le n$
d_t	diameter of nanotube	$d_t = \frac{L}{\pi} = \frac{\sqrt{n^2 + m^2 + nm}}{\pi}a$	
θ	chiral angle	$\sin\theta = \frac{\sqrt{3}m}{2\sqrt{n^2 + m^2 + nm}}$	$0 \le \lvert\theta\rvert \le 30°$
		$\cos\theta = \frac{2n + m}{2\sqrt{n^2 + m^2 + nm}}$	
		$\tan\theta = \frac{\sqrt{3}m}{2n + m}$	
d	the highest common divisor of (n,m)		
d_R	the highest common divisor of $(2n + m, 2m + n)$	$d_R = \begin{cases} d & \text{if } n - m \text{ not a multiple of } 3d \\ 3d & \text{if } n - m \text{ a multiple of } 3d. \end{cases}$	
$\mathbf{T}$	translational vector of 1D unit cell	$\mathbf{T} = t_1\mathbf{a}_1 + t_2\mathbf{a}_2 \equiv (t_1, t_2)$	t_1, t_2: integers
		$t_1 = \frac{2m + n}{d_R}$	
		$t_2 = -\frac{2n + m}{d_R}$	
T	length of $\mathbf{T}$	$T = \frac{\sqrt{3}L}{d_R}$	
N	number of hexagons per 1D unit cell	$N = \frac{2(n^2 + m^2 + nm)}{d_R}$	$2N \equiv n_C$/unit cell
$\mathbf{R}$	symmetry vector‡	$\mathbf{R} = p\mathbf{a}_1 + q\mathbf{a}_2 \equiv (p,q)$	p,q: integers†
		$d = mp - nq,\ 0 \le p \le n/d,\ 0 \le q \le m/d$	
M	number of 2π revolutions	$M = [(2n + m)p + (2m + n)q]/d_R$	M: integer
		$N\mathbf{R} = M\mathbf{C}_h + d\mathbf{T}$	
R	basic symmetry operation‡	$R = (\psi\,\vert\,\tau)$	
ψ	rotation operation	$\psi = 2\pi\frac{M}{N}, \left(\chi = \frac{\psi L}{2\pi}\right)$	ψ: radians
τ	translation operation	$\tau = \frac{d\mathbf{T}}{N}$	τ,χ: length

† (p,q) are uniquely determined by $d = mp - nq$, subject to conditions stated in table, except for zigzag tubes for which $\mathbf{C}_h = (n,0)$, and we define $p = 1$, $q = -1$, which gives $M = 1$.

‡ $\mathbf{R}$ and R refer to the same symmetry operation.

$(n,0)$ tubules], where the translational and rotational symmetry operations can each be executed independently, or the symmetry group can be non-symmorphic (for a general nanotube), where the basic symmetry operations require both a rotation ψ and translation τ and is written as $R = (\psi\,|\,\tau)$[7]. We consider the symmorphic case in some detail in this article, and refer the reader to the paper by Eklund *et al.*[8] in this volume for further details regarding the non-symmorphic space groups for chiral nanotubes.

The symmetry operations of the infinitely long armchair tubule ($n = m$), or zigzag tubule ($m = 0$), are described by the symmetry groups D_{nh} or D_{nd} for even or odd n, respectively, since inversion is an element of D_{nd} only for odd n, and is an element of D_{nh} only for even n[9]. Character tables for the D_n groups

Table 2. Values for characterization parameters for selected carbon nanotubes labeled by (n,m)[7]

(n,m)	d	d_R	d_t (Å)	L/a	T/a	N	$\psi/2\pi$	τ/a	M
(5,5)	5	15	6.78	$\sqrt{75}$	1	10	1/10	1/2	1
(9,0)	9	9	7.05	9	$\sqrt{3}$	18	1/18	$\sqrt{3}/2$	1
(6,5)	1	1	7.47	$\sqrt{91}$	$\sqrt{273}$	182	149/182	$\sqrt{3/364}$	149
(7,4)	1	3	7.55	$\sqrt{93}$	$\sqrt{31}$	62	17/62	$1/\sqrt{124}$	17
(8,3)	1	1	7.72	$\sqrt{97}$	$\sqrt{291}$	194	71/194	$\sqrt{3/388}$	71
(10,0)	10	10	7.83	10	$\sqrt{3}$	20	1/20	$\sqrt{3}/2$	1
(6,6)	6	18	8.14	$\sqrt{108}$	1	12	1/12	1/2	1
10,5)	5	5	10.36	$\sqrt{175}$	$\sqrt{21}$	70	1/14	$\sqrt{3/28}$	5
(20,5)	5	15	17.95	$\sqrt{525}$	$\sqrt{7}$	70	3/70	$1/(\sqrt{28})$	3
(30,15)	15	15	31.09	$\sqrt{1575}$	$\sqrt{21}$	210	1/42	$\sqrt{3/28}$	5
⋮	⋮	⋮	⋮	⋮	⋮	⋮	⋮	⋮	⋮
(n,n)	n	$3n$	$\sqrt{3}na/\pi$	$\sqrt{3}n$	1	$2n$	$1/2n$	1/2	1
$(n,0)$	n	n	na/π	n	$\sqrt{3}$	$2n$	$1/2n$	$\sqrt{3}/2$	1

are given in Table 3 (for odd $n = 2j + 1$) and in Table 4 (for even $n = 2j$), where j is an integer. Useful basis functions are listed in Table 5 for both the symmorphic groups (D_{2j} and D_{2j+1}) and non-symmorphic groups $C_{N/\Omega}$ discussed by Eklund *et al.*[8].

Upon taking the direct product of group D_n with the inversion group which contains two elements (E,i), we can construct the character tables for $D_{nd} = D_n \otimes i$ from Table 3 to yield D_{5d}, D_{7d}, ... for symmorphic tubules with odd numbers of unit cells around the circumference [(5,5), (7,7), ... armchair tubules and (9,0), (11,0), ... zigzag tubules]. Likewise, the character table for $D_{nh} = D_n \otimes \sigma_h$ can be obtained from Table 4 to yield D_{6h}, D_{8h}, ... for even n. Table 4 shows two additional classes for group D_{2j} relative to group $D_{(2j+1)}$, because rotation by π about the main symmetry axis is in a class by itself for groups D_{2j}. Also the n two-fold axes nC_2' form a class and represent two-fold rotations in a plane normal to the main symmetry axis $C_{\phi j}$, while the nC_2'' dihedral axes, which are bisectors of the nC_2' axes, also form a class for group D_n when n is an even integer. Correspondingly, there are two additional one-dimensional representations B_1 and B_2 in D_{2j} corresponding to the two additional classes cited above.

The symmetry groups for the chiral tubules are Abelian groups. The corresponding space groups are non-symmorphic and the basic symmetry operations

Table 3. Character table for group $D_{(2j+1)}$

$\mathfrak{R}$	E	$2C_{\phi_j}^1$	$2C_{\phi_j}^2$	...	$2C_{\phi_j}^j$	$(2j+1)C_2'$
A_1	1	1	1	...	1	1
A_2	1	1	1	...	1	−1
E_1	2	$2\cos\phi_j$	$2\cos 2\phi_j$	...	$2\cos j\phi_j$	0
E_2	2	$2\cos 2\phi_j$	$2\cos 4\phi_j$	...	$2\cos 2j\phi_j$	0
⋮	⋮	⋮	⋮	⋮	⋮	⋮
E_j	2	$2\cos j\phi_j$	$2\cos 2j\phi_j$	...	$2\cos j^2\phi_j$	0

where $\phi_j = 2\pi/(2j + 1)$ and j is an integer.

$R = (\psi|\tau)$ require translations τ in addition to rotations ψ. The irreducible representations for all Abelian groups have a phase factor ϵ, consistent with the requirement that all h symmetry elements of the symmetry group commute. These symmetry elements of the Abelian group are obtained by multiplication of the symmetry element $R = (\psi|\tau)$ by itself an appropriate number of times, since $R^h = E$, where E is the identity element, and h is the number of elements in the Abelian group. We note that N, the number of hexagons in the 1D unit cell of the nanotube, is not always equal h, particularly when $d \neq 1$ and $d_R \neq d$.

To find the symmetry operations for the Abelian group for a carbon nanotube specified by the (n,m) integer pair, we introduce the basic symmetry vector $\mathbf{R} = p\mathbf{a}_1 + q\mathbf{a}_2$, shown in Fig. 4, which has a very important physical meaning. The projection of $\mathbf{R}$ on the $\mathbf{C}_h$ axis specifies the angle of rotation ψ in the basic symmetry operation $R = (\psi|\tau)$, while the projection of $\mathbf{R}$ on the $\mathbf{T}$ axis specifies the translation τ. In Fig. 4 the rotation angle ψ is shown as $\chi = \psi L/2\pi$. If we translate $\mathbf{R}$ by (N/d) times, we reach a lattice point B'' (see Fig. 4). This leads to the relation $N\mathbf{R} = M\mathbf{C}_h + d\mathbf{T}$ where the integer M is interpreted as the integral number of 2π cycles of rotation which occur after N rotations of ψ. Explicit relations for $\mathbf{R}$, ψ, and τ are contained in Table 1. If d the largest common divisor of (n,m) is an integer greater than 1, than (N/d) translations of $\mathbf{R}$ will translate the origin O to a lattice point B'', and the projection $(N/d)\mathbf{R}\cdot\mathbf{T} = T^2$. The total rotation angle ψ then becomes $2\pi(M/d)$ when $(N/d)\mathbf{R}$ reaches a lattice point B''. Listed in Table 2 are values for several representative carbon nanotubes for the rotation angle ψ in units of 2π, and the translation length τ in units of lattice constant a for the graphene layer, as well as values for M.

From the symmetry operations $R = (\psi|\tau)$ for tubules (n,m), the non-symmorphic symmetry group of the chiral tubule can be determined. Thus, from a symmetry standpoint, a carbon tubule is a one-dimensional crystal with a translation vector $\mathbf{T}$ along the cylinder axis, and a small number N of carbon

Table 4. Character table for group $D_{(2j)}$

$\mathcal{R}$	E	C_2	$2C_{\phi_j}^1$	$2C_{\phi_j}^2$	...	$2C_{\phi_j}^{j-1}$	$(2j)C_2'$	$(2j)C_2''$
A_1	1	1	1	1	...	1	1	1
A_2	1	1	1	1	...	1	−1	−1
B_1	1	−1	1	1	...	1	1	−1
B_2	1	−1	1	1	...	1	−1	1
E_1	2	−2	$2\cos\phi_j$	$2\cos 2\phi_j$	...	$2\cos(j-1)\phi_j$	0	0
E_2	2	2	$2\cos 2\phi_j$	$2\cos 4\phi_j$	...	$2\cos 2(j-1)\phi_j$	0	0
⋮	⋮	⋮	⋮	⋮	⋮	⋮	⋮	⋮
E_{j-1}	2	$(-1)^{j-1}2$	$2\cos(j-1)\phi_j$	$2\cos 2(j-1)\phi_j$	...	$2\cos(j-1)^2\phi_j$	0	0

where $\phi_j = 2\pi/(2j)$ and j is an integer.

hexagons associated with the 1D unit cell. The phase factor ϵ for the nanotube Abelian group becomes $\epsilon = \exp(2\pi iM/N)$ for the case where (n,m) have no common divisors (i.e., $d = 1$). If $M = 1$, as for the case of zigzag tubules as in Fig. 2(b) $N\mathbf{R}$ reach a lattice point after a 2π rotation.

As seen in Table 2, many of the chiral tubules with $d = 1$ have large values for M; for example, for the (6,5) tubule, $M = 149$, while for the (7,4) tubule, $M = 17$. Thus, many 2π rotations around the tubule axis are needed in some cases to reach a lattice point of the 1D lattice. A more detailed discussion of the symmetry properties of the non-symmorphic chiral groups is given elsewhere in this volume[8].

Because the 1D unit cells for the symmorphic groups are relatively small in area, the number of phonon branches or the number of electronic energy bands associated with the 1D dispersion relations is relatively small. Of course, for the chiral tubules the 1D unit cells are very large, so that the number of phonon branches and electronic energy bands is also large. Using the transformation properties of the atoms within the unit cell ($\chi^{\text{atom sites}}$) and the transformation properties of the 1D unit cells that form an Abelian group, the symmetries for the dispersion relations for phonon are obtained[9,10]. In the case of π energy bands, the number and symmetries of the distinct energy bands can be obtained by the decomposition of the equivalence transformation ($\chi^{\text{atom sites}}$) for the atoms for the 1D unit cell using the irreducible representations of the symmetry group.

Table 5. Basis functions for groups $D_{(2j)}$ and $D_{(2j+1)}$

Basis function		$D_{(2j)}$	$D_{(2j+1)}$	$C_{N/\Omega}$
(x^2+y^2, z^2)		A_1	A_1	A
	z	A_2	A_1	A
	R_z	A_2	A_2	A
(xz, yz)	(x,y)	E_1	E_1	E_1
(x^2-y^2, xy)	(R_x, R_y)	E_2	E_2	E_2
		⋮	⋮	⋮

We illustrate some typical results below for electrons and phonons. Closely related results are given elsewhere in this volume[8,11].

The phonon dispersion relations for $(n,0)$ zigzag tubules have $4 \times 3n = 12n$ degrees of freedom with 60 phonon branches, having the symmetry types (for n odd, and D_{nd} symmetry):

$$\begin{aligned}\Gamma_n^{\text{vib}} = {} & 3A_{1g} + 3A_{1u} + 3A_{2g} + 3A_{2u} \\ & + 6E_{1g} + 6E_{1u} + 6E_{2g} + 6E_{2u} \\ & + \ldots + 6E_{[(n-1)/2]g} + 6E_{[(n-1)/2]u}.\end{aligned} \tag{1}$$

Of these many modes there are only 7 nonvanishing modes which are infrared-active ($2A_{2u} + 5E_{1u}$) and 15 modes that are Raman-active. Thus, by increasing the diameter of the zigzag tubules, modes with different symmetries are added, though the number and symmetry of the optically active modes remain the

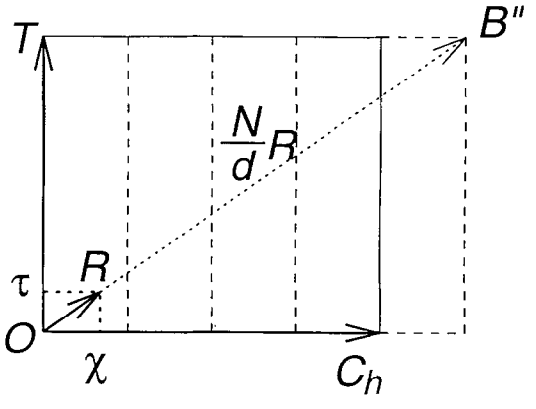

Fig. 4. The relation between the fundamental symmetry vector $\mathbf{R} = p\mathbf{a}_1 + q\mathbf{a}_2$ and the two vectors of the tubule unit cell for a carbon nanotube specified by (n,m) which, in turn, determine the chiral vector $\mathbf{C}_h$ and the translation vector $\mathbf{T}$. The projection of $\mathbf{R}$ on the $\mathbf{C}_h$ and $\mathbf{T}$ axes, respectively, yield ψ (or χ) and τ (see text). After (N/d) translations, $\mathbf{R}$ reaches a lattice point B''. The dashed vertical lines denote normals to the vector $\mathbf{C}_h$ at distances of $L/d, 2L/d, 3L/d, \ldots, L$ from the origin.

same. This is a symmetry-imposed result that is generally valid for all carbon nanotubes.

Regarding the electronic structure, the number of energy bands for $(n,0)$ zigzag carbon nanotubes is $2n$, the number of carbon atoms per unit cell, with symmetries

$$\chi_n^{\text{electronic}} = A_{1g} + A_{1u} + A_{2g} + A_{2u} + 2E_{1g} + 2E_{1u} + 2E_{2g} + 2E_{2u} + \ldots + 2E_{[(n-1/2]g} + 2E_{[(n-1)/2]u}. \quad (2)$$

A symmetry-imposed band degeneracy occurs for the $E_{[(n-3)/2]g}$ and $E_{[(n-3/2]u}$ bands at the Fermi level, when $n = 3r$, r being an integer, thereby giving rise to zero gap tubules with metallic conduction. On the other hand, when $n \neq 3r$, a bandgap and semiconducting behavior results. Independent of whether the tubules are conducting or semiconducting, each of the $[4 + 2(n-1)]$ energy bands is expected to show a $(E - E_0)^{-1/2}$ type singularity in the density of states at its band extremum energy E_0[10].

The most promising present technique for carrying out sensitive measurements of the electronic properties of individual tubules is scanning tunneling spectroscopy (STS) because of the ability of the tunneling tip to probe most sensitively the electronic density of states of either a single-wall nanotube[12], or the outermost cylinder of a multi-wall tubule or, more generally, a bundle of tubules. With this technique, it is further possible to carry out both STS and scanning tunneling microscopy (STM) measurements at the same location on the same tubule and, therefore, to measure the tubule diameter concurrently with the STS spectrum.

Although still preliminary, the study that provides the most detailed test of the theory for the electronic properties of the 1D carbon nanotubes, thus far, is the combined STM/STS study by Olk and Heremans[13]. In this STM/STS study, more than nine individual multilayer tubules with diameters ranging from 1.7 to 9.5 nm were examined. The *I-V* plots provide evidence for both metallic and semiconducting tubules[13,14]. Plots of dI/dV indicate maxima in the 1D density of states, suggestive of predicted singularities in the 1D density of states for carbon nanotubes. This STM/STS study further shows that the energy gap for the semiconducting tubules is proportional to the inverse tubule diameter $1/d_t$, and is independent of the tubule chirality.

4. MULTI-WALL NANOTUBES AND ARRAYS

Much of the experimental observations on carbon nanotubes thus far have been made on multi-wall tubules[15–19]. This has inspired a number of theoretical calculations to extend the theoretical results initially obtained for single-wall nanotubes to observations in multilayer tubules. These calculations for multi-wall tubules have been informative for the interpretation of experiments, and influential for suggesting new research directions. The multi-wall calculations have been predominantly done for double-wall tubules, although some calculations have been done for a four-walled tubule[16–18] and also for nanotube arrays [16,17].

The first calculation for a double-wall carbon nanotube[15] was done using the tight binding technique, which sensitively includes all symmetry constraints in a simplified Hamiltonian. The specific geometrical arrangement that was considered is the most commensurate case possible for a double-layer nanotube, for which the ratio of the chiral vectors for the two layers is 1:2, and in the direction of translational vectors, the ratio of the lengths is 1:1. Because the C_{60}-derived tubule has a radius of 3.4 Å, which is close to the interlayer distance for turbostratic graphite, this geometry corresponds to the minimum diameter for a double-layer tubule. This geometry has many similarities to the AB stacking of graphite. In the double-layer tubule with the diameter ratio 1:2, the interlayer interaction γ_1 involves only half the number of carbon atoms as in graphite, because of the smaller number of atoms on the inner tubule. Even though the geometry was chosen to give rise to the most commensurate interlayer stacking, the energy dispersion relations are only weakly perturbed by the interlayer interaction.

More specifically, the calculated energy band structure showed that two coaxial zigzag nanotubes that would each be metallic as single-wall nanotubes yield a metallic double-wall nanotube when a weak interlayer coupling between the concentric nanotubes is introduced. Similarly, two coaxial semiconducting tubules remain semiconducting when the weak interlayer coupling is introduced[15]. More interesting is the case of coaxial metal-semiconductor and semiconductor-metal nanotubes, which also retain their individual metallic and semiconducting identities when the weak interlayer interaction is turned on. On the basis of this result, we conclude that it might be possible to prepare metal-insulator device structures in the coaxial geometry without introducing any doping impurities[20], as has already been suggested in the literature[10,20,21].

A second calculation was done for a two-layer tubule using density functional theory in the local density approximation to establish the optimum interlayer distance between an inner (5,5) armchair tubule and an outer armchair (10,10) tubule. The result of this calculation yielded a 3.39 Å interlayer separation [16,17], with an energy stabilization of 48 meV/carbon atom. The fact that the interlayer separation is about halfway between the graphite value of 3.35 Å and the 3.44 Å separation expected for turbostratic graphite may be explained by interlayer correlation between the carbon atom sites both along the tubule axis direction and circumferentially. A similar calculation for double-layered hyper-fullerenes has also been carried out, yielding an interlayer spacing of 3.524 Å for $C_{60}@C_{240}$ with an energy stabilization of 14 meV/C atom for this case[22]. In the case of the double-layered hyper-fullerene, there is a greatly reduced pos-

sibility for interlayer correlations, even if C_{60} and C_{240} take the same I_h axes. Further, in the case of C_{240}, the molecule deviates from a spherical shape to an icosahedron shape. Because of the curvature, it is expected that the spherically averaged interlayer spacing between the double-layered hyper-fullerenes is greater than that for turbostratic graphite.

In addition, for two coaxial armchair tubules, estimates for the translational and rotational energy barriers (of 0.23 meV/atom and 0.52 meV/atom, respectively) were obtained, suggesting significant translational and rotational interlayer mobility of ideal tubules at room temperature[16,17]. Of course, constraints associated with the cap structure and with defects on the tubules would be expected to restrict these motions. The detailed band calculations for various interplanar geometries for the two coaxial armchair tubules basically confirm the tight binding results mentioned above[16,17].

Further calculations are needed to determine whether or not a Peierls distortion might remove the coaxial nesting of carbon nanotubes. Generally 1D metallic bands are unstable against weak perturbations which open an energy gap at E_F and consequently lower the total energy, which is known as the Peierls instability[23]. In the case of carbon nanotubes, both in-plane and out-of-plane lattice distortions may couple with the electrons at the Fermi energy. Mintmire and White have discussed the case of in-plane distortion and have concluded that carbon nanotubes are stable against a Peierls distortion in-plane at room temperature[24], though the in-plane distortion, like a Kekulé pattern, will be at least 3 times as large a unit cell as that of graphite. The corresponding chiral vectors satisfy the condition for metallic conduction ($n - m = 3r, r$:integer). However, if we consider the direction of the translational vector **T**, a symmetry-lowering distortion is not always possible, consistent with the boundary conditions for the general tubules[25]. On the other hand, out-of-plane vibrations do not change the size of the unit cell, but result in a different site energy for carbon atoms on A and B sites for carbon nanotube structures[26]. This situation is applicable, too, if the dimerization is of the "quinone" or chain-like type, where out-of-plane distortions lead to a perturbation approaching the limit of 2D graphite. Further, Harigaya and Fujita[27,28] showed that an in-plane alternating double-single bond pattern for the carbon atoms within the 1D unit cell is possible only for several choices of chiral vectors.

Solving the self-consistent calculation for these types of distortion, an energy gap is always opened by the Peierls instability. However, the energy gap is very small compared with that of normal 1D cosine energy bands. The reason why the energy gap for 1D tubules is so small is that the energy gain comes from only one of the many 1D energy bands, while the energy loss due to the distortion affects all the 1D energy bands. Thus, the Peierls energy gap decreases exponentially with increasing number of energy bands N[24,26–28]. Because the energy change due to the Peierls distortion is zero in the limit of 2D graphite, this result is consistent with the limiting case of $N = \infty$. This very small Peierls gap is, thus, negligible at finite temperatures and in the presence of fluctuations arising from 1D conductors. Very recently, Viet *et al.* showed[29] that the in-plane and out-of-plane distortions do not occur simultaneously, but their conclusions regarding the Peierls gap for carbon nanotubes are essentially as discussed above.

The band structure of four concentric armchair tubules with 10, 20, 30, and 40 carbon atoms around their circumferences (external diameter 27.12 Å) was calculated, where the tubules were positioned to minimize the energy for all bilayered pairs[17]. In this case, the four-layered tubule remains metallic, similar to the behavior of two double-layered armchair nanotubes, except that tiny band splittings form.

Inspired by experimental observations on bundles of carbon nanotubes, calculations of the electronic structure have also been carried out on arrays of (6,6) armchair nanotubes to determine the crystalline structure of the arrays, the relative orientation of adjacent nanotubes, and the optimal spacing between them. Figure 5 shows one tetragonal and two hexagonal arrays that were considered, with space group symmetries $P4_2/mmc$ (D^9_{4h}), $P6/mmm$ (D^1_{6h}), and $P6/mcc$ (D^2_{6h}), respectively[16,17,30]. The calculation shows

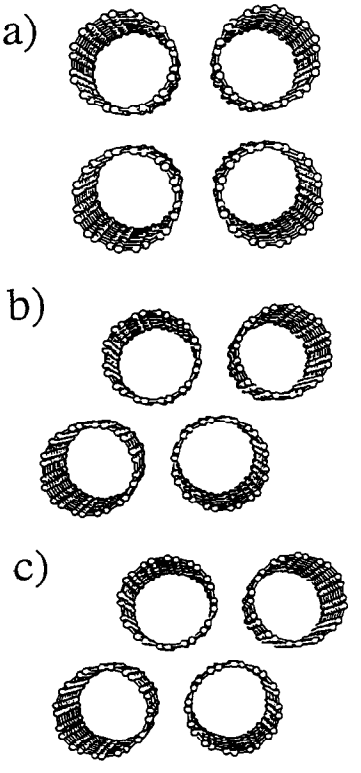

Fig. 5. Schematic representation of arrays of carbon nanotubes with a common tubule axial direction in the (a) tetragonal, (b) hexagonal I, and (c) hexagonal II arrangements. The reference nanotube is generated using a planar ring of twelve carbon atoms arranged in six pairs with the D_{6h} symmetry [16,17,30].

that the hexagonal $P6/mcc$ (D_{6h}^2) space group has the lowest energy, leading to a gain in cohesive energy of 2.4 meV/C atom. The orientational alignment between tubules leads to an even greater gain in cohesive energy (3.4 eV/C atom). The optimal alignment between tubules relates closely to the ABAB stacking of graphite, with an inter-tubule separation of 3.14 Å at closest approach, showing that the curvature of the tubules lowers the minimum interplanar distance (as is also found for fullerenes where the corresponding distance is 2.8 Å). The importance of the inter-tubule interaction can be seen in the reduction in the inter-tubule closest approach distance to 3.14 Å for the $P6/mcc$ (D_{6h}^2) structure, from 3.36 Å and 3.35 Å, respectively, for the tetragonal $P4_2/mmc$ (D_{4h}^9) and $P6/mmm$ (D_{6h}^1) space groups. A plot of the electron dispersion relations for the most stable case is given in Fig. 6[16,17,30], showing the metallic nature of this tubule array by the degeneracy point between the H and K points in the Brillouin zone between the valence and conduction bands. It is expected that further calculations will consider the interactions between nested nanotubes having different symmetries, which on physical grounds should interact more weakly, because of a lack of correlation between near neighbors.

Modifications of the conduction properties of semiconducting carbon nanotubes by B (p-type) and N (n-type) substitutional doping has also been discussed[31] and, in addition, electronic modifications by filling the capillaries of the tubes have also been proposed[32]. Exohedral doping of the space between nanotubes in a tubule bundle could provide yet another mechanism for doping the tubules. Doping of the nanotubes by insertion of an intercalate species between the layers of the tubules seems unfavorable because the interlayer spacing is too small to accommodate an intercalate layer without fracturing the shells within the nanotube.

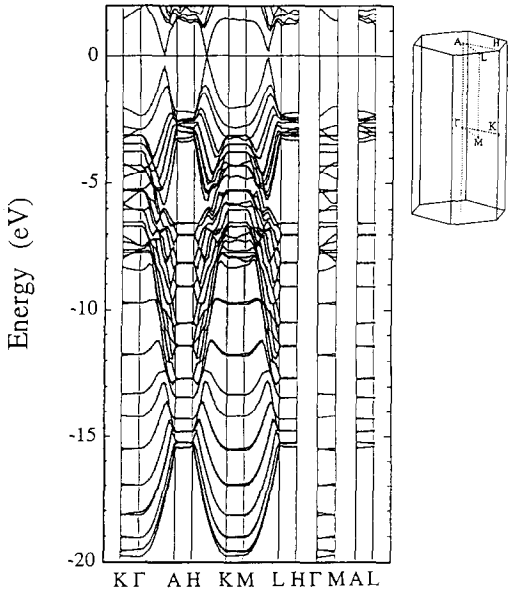

Fig. 6. Self-consistent band structure (48 valence and 5 conduction bands) for the hexagonal II arrangement of nanotubes, calculated along different high-symmetry directions in the Brillouin zone. The Fermi level is positioned at the degeneracy point appearing between K-H, indicating metallic behavior for this tubule array[17].

No superconductivity has yet been found in carbon nanotubes or nanotube arrays. Despite the prediction that 1D electronic systems cannot support superconductivity[33,34], it is not clear that such theories are applicable to carbon nanotubes, which are tubular with a hollow core and have several unit cells around the circumference. Doping of nanotube bundles by the insertion of alkali metal dopants between the tubules could lead to superconductivity. The doping of individual tubules may provide another possible approach to superconductivity for carbon nanotube systems.

5. DISCUSSION

This journal issue features the many unusual properties of carbon nanotubes. Most of these unusual properties are a direct consequence of their 1D quantum behavior and symmetry properties, including their unique conduction properties[11] and their unique vibrational spectra[8].

Regarding electrical conduction, carbon nanotubes show the unique property that the conductivity can be either metallic or semiconducting, depending on the tubule diameter d_t and chiral angle θ. For carbon nanotubes, metallic conduction can be achieved without the introduction of doping or defects. Among the tubules that are semiconducting, their band gaps appear to be proportional to $1/d_t$, independent of the tubule chirality. Regarding lattice vibrations, the number of vibrational normal modes increases with increasing diameter, as expected. Nevertheless, following from the 1D symmetry properties of the nanotubes, the number of infrared-active and Raman-active modes remains independent of tubule diameter, though the vibrational frequencies for these optically active modes are sensitive to tubule diameter and chirality[8]. Because of the restrictions on momentum transfer between electrons and phonons in the electron-phonon interaction for carbon nanotubes, it has been predicted that the interaction between electrons and longitudinal phonons gives rise only to intraband scattering and not interband scattering. Correspondingly, the interaction between electrons and transverse phonons gives rise only to interband electron scattering and not to intraband scattering[35].

These properties are illustrative of the unique behavior of 1D systems on a rolled surface and result from the group symmetry outlined in this paper. Observation of 1D quantum effects in carbon nanotubes requires study of tubules of sufficiently small diameter to exhibit measurable quantum effects and, ideally, the measurements should be made on single nanotubes, characterized for their diameter and chirality. Interesting effects can be observed in carbon nanotubes for diameters in the range 1–20 nm, depending

on the property under investigation. To see 1D effects, faceting should be avoided, insofar as facets lead to 2D behavior, as in graphite. To emphasize the possibility of semiconducting properties in non-defective carbon nanotubes, and to distinguish between conductors and semiconductors of similar diameter, experiments should be done on nanotubes of the smallest possible diameter. To demonstrate experimentally the high density of electronic states expected for 1D systems, experiments should ideally be carried out on single-walled tubules of small diameter. However, to demonstrate magnetic properties in carbon nanotubes with a magnetic field normal to the tubule axis, the tubule diameter should be large compared with the Landau radius and, in this case, a tubule size of ~10 nm would be more desirable, because the magnetic localization within the tubule diameter would otherwise lead to high field graphitic behavior.

The ability of experimentalists to study 1D quantum behavior in carbon nanotubes would be greatly enhanced if the purification of carbon tubules in the synthesis process could successfully separate tubules of a given diameter and chirality. A new method for producing mass quantities of carbon nanotubes under controlled conditions would be highly desirable, as is now the case for producing commercial quantities of carbon fibers. It is expected that nano-techniques for manipulating very small quantities of material of nm size[14,36] will be improved through research of carbon nanotubes, including research capabilities involving the STM and AFM techniques. Also of interest will be the bonding of carbon nanotubes to the other surfaces, and the preparation of composite or multilayer systems that involve carbon nanotubes. The unbelievable progress in the last 30 years of semiconducting physics and devices inspires our imagination about future progress in 1D systems, where carbon nanotubes may become a benchmark material for study of 1D systems about a cylindrical surface.

Acknowledgements—We gratefully acknowledge stimulating discussions with T. W. Ebbesen, M. Endo, and R. A. Jishi. We are also in debt to many colleagues for assistance. The research at MIT is funded by NSF grant DMR-92-01878. One of the authors (RS) acknowledges the Japan Society for the Promotion of Science for supporting part of his joint research with MIT. Part of the work by RS is supported by a Grant-in-Aid for Scientific Research in Priority Area "Carbon Cluster" (Area No. 234/05233214) from the Ministry of Education, Science and Culture, Japan.

REFERENCES

1. S. Iijima, *Nature* (London) **354**, 56 (1991).
2. T. W. Ebbesen and P. M. Ajayan, *Nature* (London) **358**, 220 (1992).
3. T. W. Ebbesen, H. Hiura, J. Fujita, Y. Ochiai, S. Matsui, and K. Tanigaki, *Chem. Phys. Lett.* **209**, 83 (1993).
4. D. S. Bethune, C. H. Kiang, M. S. de Vries, G. Gorman, R. Savoy, J. Vazquez, and R. Beyers, *Nature* (London) **363**, 605 (1993).
5. S. Iijima and T. Ichihashi, *Nature* (London) **363**, 603 (1993).
6. M. S. Dresselhaus, G. Dresselhaus, and R. Saito, *Phys. Rev. B* **45**, 6234 (1992).
7. R. A. Jishi, M. S. Dresselhaus, and G. Dresselhaus, *Phys. Rev. B* **47**, 16671 (1993).
8. P. C. Eklund, J. M. Holden, and R. A. Jishi, *Carbon* **33**, 959 (1995).
9. R. A. Jishi, L. Venkataraman, M. S. Dresselhaus, and G. Dresselhaus, *Chem. Phys. Lett.* **209**, 77 (1993).
10. Riichiro Saito, Mitsutaka Fujita, G. Dresselhaus, and M. S. Dresselhaus, *Mater. Sci. Engin.* **B19**, 185 (1993).
11. J. W. Mintmire and C. T. White, *Carbon* **33**, 893 (1995).
12. S. Wang and D. Zhou, *Chem. Phys. Lett.* **225**, 165 (1994).
13. C. H. Olk and J. P. Heremans, *J. Mater. Res.* **9**, 259 (1994).
14. J. P. Issi *et al.*, *Carbon* **33**, 941 (1995).
15. R. Saito, G. Dresselhaus, and M. S. Dresselhaus, *J. Appl. Phys.* **73**, 494 (1993).
16. J. C. Charlier and J. P. Michenaud, *Phys. Rev. Lett.* **70**, 1858 (1993).
17. J. C. Charlier, *Carbon Nanotubes and Fullerenes*. PhD thesis, Catholic University of Louvain, Department of Physics, May 1994.
18. Ph. Lambin, L. Philippe, J. C. Charlier, and J. P. Michenaud, *Comput. Mater. Sci.* **2**, 350 (1994).
19. Ph. Lambin, L. Philippe, J. C. Charlier, and J. P. Michenaud, In *Proceedings of the Winter School on Fullerenes* (Edited by H. Kuzmany, J. Fink, M. Mehring, and S. Roth), Kirchberg Winter School, Singapore, World Scientific Publishing Co., Ltd. (1994).
20. R. Saito, M. Fujita, G. Dresselhaus, and M. S. Dresselhaus, *Appl. Phys. Lett.* **60**, 2204 (1992).
21. M. S. Dresselhaus, G. Dresselhaus, and Riichiro Saito, *Mater. Sci. Engin.* **B19**, 122 (1993).
22. Y. Yosida, *Fullerene Sci. Tech.* **1**, 55 (1993).
23. R. E. Peierls, In *Quantum Theory of Solids*. London, Oxford University Press (1955).
24. J. W. Mintmire, *Phys. Rev B* **43**, 14281 (June 1991).
25. Kikuo Harigaya, *Chem. Phys. Lett.* **189**, 79 (1992).
26. R. Saito, M. Fujita, G. Dresselhaus, and M. S. Dresselhaus, In *Electrical, Optical and Magnetic Properties of Organic Solid State Materials, MRS Symposia Proceedings, Boston*. Edited by L. Y. Chiang, A. F. Garito, and D. J. Sandman, vol. 247, p. 333, Pittsburgh, PA, Materials Research Society Press (1992).
27. K. Harigaya and M. Fujita, *Phys. Rev. B* **47**, 16563 (1993).
28. K. Harigaya and M. Fujita, *Synth. Metals* **55**, 3196 (1993).
29. N. A. Viet, H. Ajiki, and T. Ando, *ISSP Technical Report* **2828** (1994).
30. J. C. Charlier, X. Gonze, and J. P. Michenaud, *Europhys. Lett.* **29**, 43 (1994).
31. J. Y. Yi and J. Bernholc, *Phys. Rev. B* **47**, 1708 (1993).
32. T. W. Ebbesen, *Annu. Rev. Mater. Sci.* **24**, 235 (1994).
33. H. Fröhlich, *Phys. Rev.* **79**, 845 (1950).
34. H. Fröhlich, *Proc. Roy. Soc. London* **A215**, 291 (1952).
35. R. A. Jishi, M. S. Dresselhaus, and G. Dresselhaus, *Phys. Rev. B* **48**, 11385 (1993).
36. L. Langer, L. Stockman, J. P. Heremans, V. Bayot, C. H. Olk, C. Van Haesendonck, Y. Bruynseraede, and J. P. Issi, *J. Mat. Res.* **9**, 927 (1994).